# Computational Determination of the Solvation Structure of LiBF<sub>4</sub> and LiPF<sub>6</sub> Salts in Battery Electrolytes

M.D. Hashan C. Peiris<sup>a</sup>, Scott Brennan<sup>a,b</sup>, Diana Liepinya<sup>c</sup>, Hao Liu<sup>a,d</sup>, Manuel Smeu<sup>a,b,\*</sup>

<sup>a</sup>Materials Science and Engineering, Binghamton University, Binghamton, NY, USA
 <sup>b</sup>Department of Physics, Binghamton University, Binghamton, NY, USA
 <sup>c</sup>Materials Science and Engineering, University of Maryland, College Park, MD, USA
 <sup>d</sup>Department of Chemistry, Binghamton University, Binghamton, NY, USA

#### Abstract

Li-ion battery technology has come a long way since its initial development a few decades ago. However, expectations of energy storage continue to grow, making the optimization of battery technology vital. Along with improving the electrochemical performance of electrodes, investigation of the properties of the electrolyte has thus become necessary. In this work, we use first principles computational modeling to investigate the structural and physical interactions of a common solvent solution, ethylene carbonate:dimethyl carbonate, with two salts, LiPF<sub>6</sub> and LiBF<sub>4</sub>. We look at how the solvation shells form and evolve using ab initio molecular dynamics (AIMD) simulations. The solvation structures extracted from the calculated trajectories are used to investigate the energetics of removal of individual solvent molecules using density functional theory (DFT). We also investigate the order in which the solvent molecules form a shell around the salts. LiBF<sub>4</sub> and LiPF<sub>6</sub> have similar solvation structures and interaction energies with the solvent, with a preference for the carbonyl oxygens and the ether oxygens to interact with the Li<sup>+</sup> cations, and the methyl or methylene groups to interact with the BF<sub>4</sub><sup>-</sup> or PF<sub>6</sub><sup>-</sup> anions. Our calculations also find that the solvation shell formed around  ${\rm LiPF}_6$  can desolvate more easily

Email address: msmeu@binghamton.edu (Manuel Smeu)

<sup>\*</sup>Corresponding author

# 1. Introduction

Rechargeable Li-ion batteries (LIBs) have emerged as the primary solution for the storage of electrical energy due to their economic viability, energy efficiency, and high reliability. Extensive utilization of battery technology for energy storage is expected to continue into the foreseeable future due to the emergence of a variety of renewable energy generation methods and climate change concerns with the general public. Moreover, the miniaturization of many electronic devices and the popularity of green vehicles necessitates the continued research and development of battery technology.

An LIB typically consists of an anode (negative electrode) made of graphite, a cathode (positive electrode) made of a LiMO<sub>2</sub>, where M is a transition metal in a layered oxide (e.g., LiCoO<sub>2</sub>), and an electrolyte with a lithium salt (e.g., LiPF<sub>6</sub>) dissolved in a mixture of alkylcarbonate organic solvents (e.g., ethylene carbonate-dimethyl carbonate, EC-DMC), one of many electrolyte configurations that have been researched and deployed commercially [1]. Other commonly used organic carbonates include mixtures of ethylene carbonate (EC) with propylene carbonate (PC), dimethoxyethane (DME), diethyl carbonate (DEC), and/or ethyl methyl carbonate (EMC) at various proportions [2, 3, 4].

The electrolyte should be stable for a specific range of temperatures for which the battery is expected to operate. Hence, the melting and boiling points of the electrolyte should be outside operating temperatures and consistent throughout its lifetime. Furthermore, due regard to operational safety and environmental friendliness in manufacturing, regular usage and end-of-life processing of electrolytes is also necessary.

During the cycling of the battery, the Li ions diffuse through the electrolyte between the cathode and the anode. While the solid electrolyte interface (SEI) is often attributed as the main layer of protection for an electrode [5, 6, 7, 8], it is dependent on the electrolyte being used and its inherent decomposition characteristics. Within the electrolytic volume, organic molecules may decompose due to interactions with water, concentration gradients with the cathode, or operating outside their thermal stability range. This decomposition can lead to a decrease in electrochemical performance [9, 10]. If the electrolyte-ion interaction is too strong, it can also result in reduced intercalation of Li ions into the electrode, as the ion needs to be able to leave the solvation shell to enter the electrode. The diffusion process is complicated by the fact that Li ions tend to form clusters of molecules known as solvation shells with the other organic solvent molecules and anions in the electrolyte. This lowers the diffusivity of the Li ions, reducing the ease with which the ion can move across the electrolyte. Additionally, solvation shells can play a large role in electrode stability [11, 12]. Therefore, a better understanding of how the electrolyte molecules interact with the Li ions is needed to optimize the performance of the battery.

Inter-ionic interactions in the salts used in electrolytes are typically identified by the arrangement of anions and cations. For electrolytes consisting of metal cations  $(M^+)$ , anions  $(X^-)$  and solvent molecules (S), these are identified as solvent shared ion pair (SIP)  $(M^+SX^-)$ , solvent separated ion pair (SSIP)  $(M^+SSX^-)$ , contact ion pair (CIP)  $(M^+X^-)$  and aggregate coordination (AGG) which can exist in various forms  $(M^+X^-M^+)$  triple ions, ion pair dimers  $(M^+X^-)_2$ , or other larger forms) (Fig. 1) [13, 14].

The solvation structure of Li<sup>+</sup> in EC/DMC solvent environments is well known, with four molecules occupying the first solvation shell [15, 16, 17, 18]. However, the solvation shell of anions is harder to study and can lead to unclear

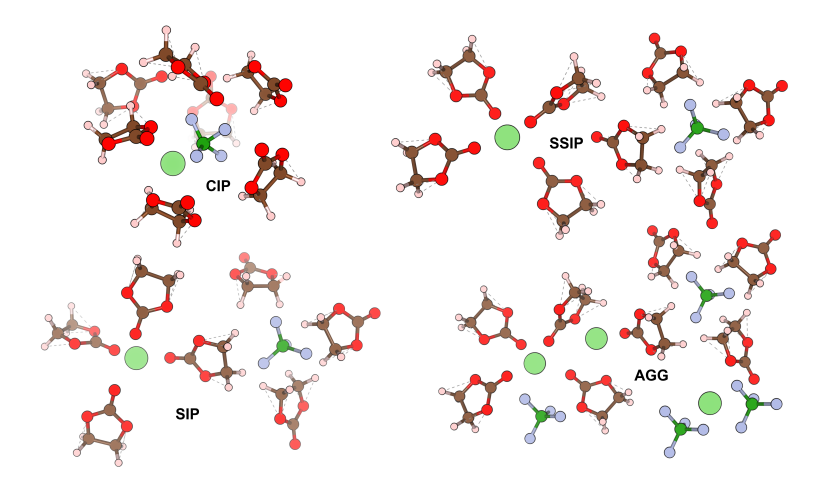


Figure 1: Common types of ion pairs found in solutions: contact ion pair (CIP), solvent shared ion pair (SIP), solvent separated ion pair (SSIP), and aggregate (AGG) shown here for  $LiBF_4$  salt dissolved in a solution of EC.

results [16, 19, 20, 21]. Chaban and coworkers used the semi-empirical PM7-MD method to study a set of neutral and negatively charged systems containing PC and DME molecules, BF<sub>4</sub><sup>-</sup> and PF<sub>6</sub><sup>-</sup> anions, and lithium cations. When in a contact ion pair with Li<sup>+</sup>, they proposed a first solvation shell for BF<sub>4</sub><sup>-</sup> to have 2.5 PC and 1.7 DME on average, and the first solvation shell of PF<sub>6</sub><sup>-</sup> to contain 2.8 PC and 1.6 DME. When studied as isolated ions, BF<sub>4</sub><sup>-</sup> was suggested to have a first solvation shell of 4.1 PC and 1.5 DME, and PF<sub>6</sub><sup>-</sup> was demonstrated to have a first solvation shell of 3.7 PC and 1.5 DME, indicating that both BF<sub>4</sub><sup>-</sup> and PF<sub>6</sub><sup>-</sup> exhibit weak binding to PC and DME molecules, resulting in the difficulty in precisely determining their first solvation shells. They also reported the preference of BF<sub>4</sub><sup>-</sup> and PF<sub>6</sub><sup>-</sup> to exist in the form of neutral ion pairs with Li<sup>+</sup> (LiPF<sub>6</sub>, LiBF<sub>4</sub>).[16]

The dynamics of the solvation shells of the LiPF<sub>6</sub> and LiBF<sub>4</sub> salts near cathode surfaces have not been studied in detail. This is often due to the difficulties in experimental investigations to distinguish surface effects and the high computational cost of using *ab initio* molecular dynamics approaches. Moreover, the

behavior of the solvation shells with respect to the state of charge of the cathode surface remains elusive. More recently, experimental attempts have been made to investigate the surface effects of cathodes have on salt solvation and battery performance [22].

In the current work, we investigated the solvation shell formed by the salts, LiPF<sub>6</sub> and LiBF<sub>4</sub>, simulating the electrolyte (1:1 EC:DMC) explicitly using an ab initio based computational modeling approach. In particular, we investigated the effects of having different salts in the electrolyte by keeping the constituents of the electrolyte consistent while varying the two CIP salt species, LiPF<sub>6</sub> or LiBF<sub>4</sub>. Determination of the formation and stability of the solvent shells was done by visualizing and analyzing the trajectories. The dynamics of the cations and anions closer to the cathode surfaces were compared, and the specific composition of anion solvation shells was determined. Multiple samples were run to improve the statistics of these results. Lastly, the formation of solvation shells of salt ions in the electrolyte was also studied by sequential addition and removal of solvents. To the best of our knowledge, this is the first theoretical investigation of the dynamics of LiPF<sub>6</sub> and LiBF<sub>4</sub> salts near LiNiO<sub>2</sub> cathode surfaces using an ab initio molecular dynamics approach.

#### 2. Methodology

This study can be broadly categorized into two phases. Firstly, the condensed phase systems were modeled where the electrolytic volume was explicitly simulated while in contact with a Ni-rich cathode (LiNiO<sub>2</sub>) using *ab initio* molecular dynamics (AIMD), enabling the observation of the formation of solvation shells with the Li ions and anions. Secondly, the simulation shells that were formed in the electrolytic region were studied as cluster models placed in a vacuum to isolate the energetics of the sequential removal and addition of

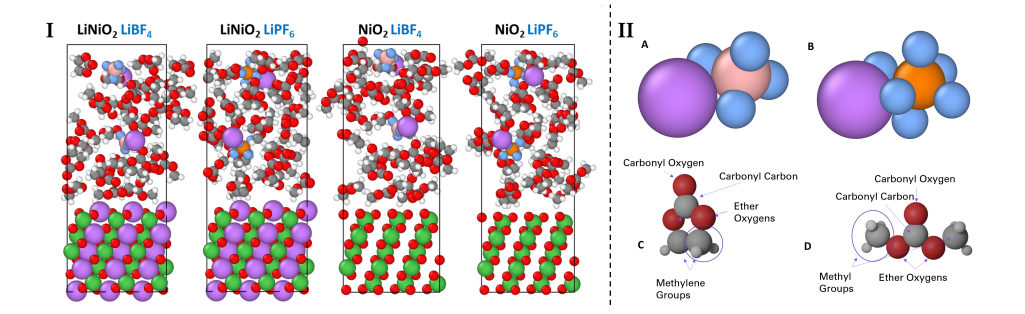


Figure 2: I. The four distinct systems with lithiated and de-lithiated Ni-rich cathodes with LiBF<sub>4</sub> and LiPF<sub>6</sub> as salts in the electrolyte. II. Initial orientations of LiBF<sub>4</sub> (A) and LiPF<sub>6</sub> (B) as placed in the systems represented by Li (purple), B (light pink), P (orange), and F (blue). Identifications of specific atoms of the EC (C) and DMC (D) molecules.

solvent molecules.

#### 2.1. Computational details

The organic electrolyte was modeled using the Vienna Ab initio Simulation Package (VASP)[23, 24, 25]. Projector augmented wave (PAW) potentials were used to mimic the ionic cores and the Perdew-Burke-Ernzerhof (PBE) generalized gradient approximation (GGA) provided the exchange and correlation functional for all structural relaxations and energy calculations [26, 27, 28, 29]. A  $\Gamma$ -centered  $1 \times 1 \times 1$  Monkhorst-Pack k-point grid was used for all calculations [30, 31]. The Brillouin zone was sampled by the use of Gaussian smearing.

All structural relaxations and energy calculations were performed using a plane wave energy cutoff set at 700 eV. The primitive cells for the cathodes were obtained from the Materials Project [32]. Setup, visualization, and manipulation of the systems were done using Ovito [33] and Vesta [34], with Avogadro [35] being used to create the electrolyte configuration.

Four distinct systems were used to model the interactions between 1:1 EC:DMC solvent and either LiBF<sub>4</sub> or LiPF<sub>6</sub> salts on both a lithiated and delithiated LiNiO<sub>2</sub> cathode, as shown in Fig. 2. Two separate trajectories were run for each system to vary starting configurations, resulting in a total of eight simula-

tions. The AIMD simulations were run at 450 K with 1-fs time steps using the canonical (NVT) ensemble [36] and were run upwards of 10 ps. This approach is typical for AIMD in the acceleration of reactions and faster equilibration. The trajectories were tested up to 750 K during the design phase and similar systems have been tested up to 800 K in recent work [2, 37, 38, 39]. This work uses a temperature regulated at 450 K as a rational approach to balance the chemical stability of the system under consideration as well as achieve a sensible trajectory under the simulated timescales. We note that the electrolyte systems were chemically stable and free from spurious effects related to temperature regulation. All the AIMD calculations were performed with a plane wave energy cutoff set at 400 eV using a  $\Gamma$ -centered k-point. Van der Waals interactions were included via the Grimme D3 approach (PBE-D3) with Becke-Johnson damping [40].

#### 2.2. Preparation of Systems used for AIMD Simulation

#### 2.2.1. Cathodes

The layered cathodes were selected such that they represent a fully lithiated (discharged)  $LiNiO_2$  (LNO) or a fully de-lithiated (charged)  $NiO_2$  (NO) state (Fig. 2). The (012) plane of the LNO and NO cathodes was used at the electrolyte-cathode interface, ensuring the periodicity of the cathode slab in two directions while serving as an active yet stable interface for interactions with the electrolyte [41].

While our calculations are motivated by high energy density Ni-rich NMC, it is not practical to model such dilute concentrations of Mn and Co due to limits on cathode size. Resultantly, we have selected LiNiO<sub>2</sub> to represent an end member of NMC-type oxides. We also consider fully delithiated NiO<sub>2</sub> in order to distinguish between reactions occurring at different stages of battery charge. We leveraged the periodic nature of the VASP simulation cells to model two

electrolyte-cathode interfaces in a single simulation as repetitive alternate layers of cathode and electrolyte at open circuit voltage (OCV). This is consistent with other studies in the literature that employ similar models without vacuum regions [2, 38, 39, 42]. Moreover, our focus in this study is the investigation of solvation structures and interactions, which are likely to be influenced by the presence of a vacuum region. The planar averaged local potential for these systems illustrates that the potential is periodic within the cathode region, changes smoothly and continuously into the electrolyte region and maintains a consistent profile within the electrolyte (Fig. S1).

## 2.2.2. Electrolytes

Table T1 in the Supporting Information (SI) summarizes the species and the number of atoms used to build the electrolyte systems. In all the systems considered for the AIMD calculation, 14 pairs of EC and DMC were placed randomly. Two salt pairs, LiPF<sub>6</sub> or LiBF<sub>4</sub>, were also added, with one closer to the cathode surface and the other placed near the center of the electrolyte volume, offering two reference points for ion behavior. The structure of the CIP salt pairs as placed in the electrolyte can be seen in Fig. 2-II.

The system volume was determined using a top-down approach, where an experimentally available concentration of 1M EC/DMC (verified using safety data sheets of commercial electrolyte solutions) was matched with the molecular concentration. The number of molecules needed to match this concentration was randomly placed inside the cell. Thereafter the system was allowed to relax using DFT before being placed alongside the cathode. Van der Waals distances for oxygen were added on both sides of the cell to account for Coulombic repulsion. This resulted in an electrolyte region with a density of  $\sim 1.28 \text{ g} \cdot \text{cm}^{-3}$ .

The equilibration of the systems is critical in MD simulations and was verified using two approaches, energy changes for a given system with respect to time.

The regulation of the temperature and electronic convergence of the calculation was closely monitored. A representative sample of the equilibration attained and temperature maintained in the system is given in Fig. S2.

Analysis of the trajectories, including but not limited to the observations of reactions, disintegration process of molecules, and inter-atomic distances was done using the cluster analysis and color-coding options in the Ovito program. Bond distances were calculated using a Python script developed in-house. The results were initially cross-checked with the Ovito software to ascertain accuracy.

Each salt was studied to determine the preferred solvation structure and the orientation of molecules in the solvation structure. The possible regions of the EC and DMC molecules considered for interaction are shown in Fig. 2, with lone pairs from the carbonyl oxygen and ether oxygen expected to interact strongly with the Li<sup>+</sup> ions.

## 2.2.3. Nearest neighbor analysis (Cumulative RDF)

A Python script was used to quantify the presence of solvation shells within the electrolyte. The script plots the frequency of atoms present near a given reference point as a function of radius from a reference atom, i.e., a radial density function (RDF). These data are presented in units of atoms present at a given radial distance summed over all timesteps (or in predefined increments) in the simulation, and it is thus termed a *cumulative* RDF. This is used to determine how long a given atom prevails around another atom at that distance, with the intensity of the peak being proportional to the duration that particular atomic distances were maintained. The bin size used in the calculations was 0.2 Å with a maximum distance range of 8 Å.

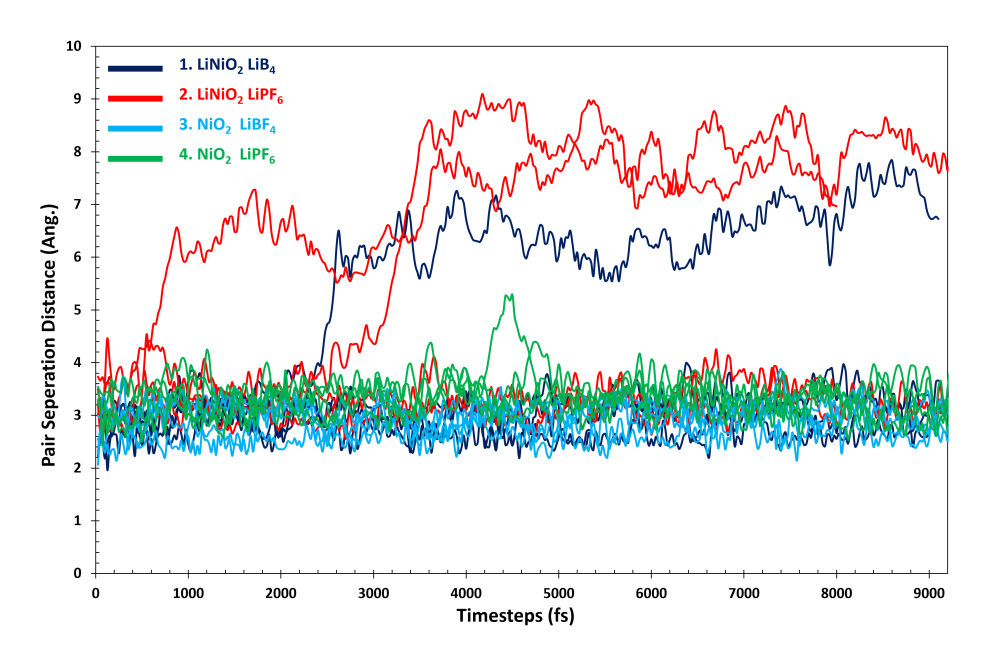


Figure 3: The cation-anion separation distance (as measured from Li to  $\rm B/P)$  as a function of time for the eight AIMD trajectories.

## 3. Results

The results are being discussed under the two approaches we used to study the behavior of the solvation shells, first from the AIMD simulation and then the DFT approach, in which we add/remove EC and DMC molecules from the solvation shell sequentially.

## 3.1. Results from the AIMD simulation

We started by investigating the formation of solvation shells in the electrolyte of the cathode-electrolyte systems (Fig. 2).

# 3.1.1. Ion pair separations

Several instances of the separation of the cation-anion pair of the salt were observed. The distance between ion pairs for all eight trajectories is illustrated in Fig. 3, displaying a total of 16 cation-anion distance plots (two ion pairs in the

electrolyte region per trajectory). The distance was measured between the Li and P/B atoms. Li<sup>+</sup> and salt anions prefer to maintain the CIP structure, with a distance of separation  $\sim 3$  Å, except for three instances where they separate close to the surface (Figs. S3 and S4 in the SI). This happened in one of the LiBF<sub>4</sub>/LiNiO<sub>2</sub> trajectories and both of the LiPF<sub>6</sub>/LiNiO<sub>2</sub> trajectories. In one of these cases, the Li<sup>+</sup> remains in the electrolyte and forms a stable solvation shell with three DMC molecules and one EC molecule. In two others, the cation and the anion descend to the cathode surface and separate. At the surface, the anions separate relatively easily and move around without constraint to any particular Li<sup>+</sup>. No separations were observed in the delithiated cathode (NiO<sub>2</sub>) simulations, with one exception. Around 4400 fs, Fig. 3 shows a transient increase in pair distance in the LiPF<sub>6</sub>/NiO<sub>2</sub> trajectory, which was revealed to be a Li<sup>+</sup> ion briefly drawn towards the surface.

In the case of a CIP shell, the highly electronegative fluorine atoms of the anions exhibit a strong preference to engage with the nearby lithium ions. However, the presence of multiple lithium ions in proximity to the fluorenes on the cathode surface allows for increased mobility and more dynamic interactions. This results in a higher propensity for the desolvation of the solvation shell at the lithiated cathode surface compared to the delithiated cathode surfaces (Fig. S5).

#### 3.1.2. Solvation shell formation and dynamics

Visualization of the trajectory revealed that the Li<sup>+</sup> in the electrolyte formed stable solvent shells lasting for a long duration (often above 5-6 ps). A previous investigation of Li<sup>+</sup> solvation shells in EC showed that typically 4 EC molecules contribute to the formation of a solvation shell when studied in a vacuum surrounding [43]. In comparison, our explicit solvent environment shows that most Li<sup>+</sup> shells consist of 2-3 solvent molecules, split evenly between EC and DMC.

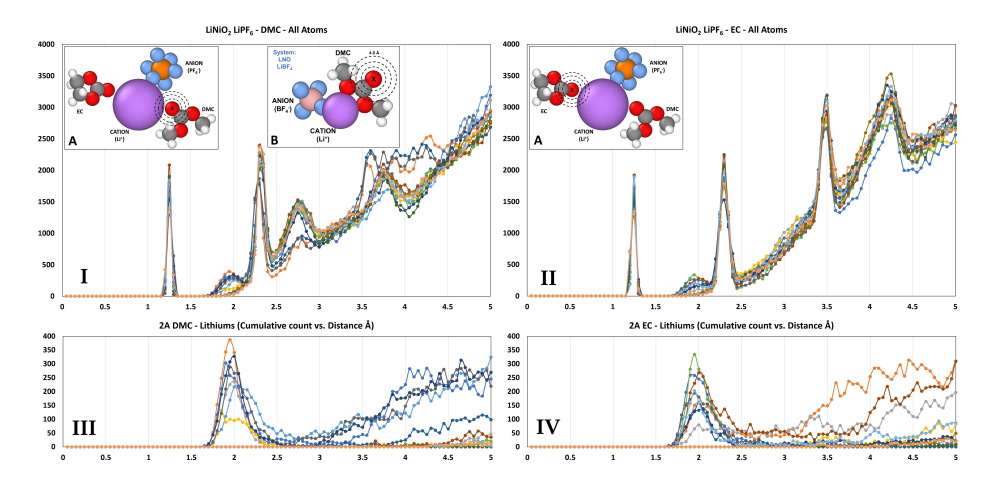


Figure 4: The representative cumulative RDF plots for carbonyl oxygen from the  ${\rm LiPF_6/LiNiO_2}$  system (I and II). Each color represents one cumulative RDF plot around a carbonyl oxygen of the solvent molecules (from DMC-left, EC-Right). The plots, III and IV, identify the carbonyl oxygen-Li<sup>+</sup> cumulative RDF plots. Inset I-A and II-A illustrate the preferred orientation of carbonyl oxygen relative to Li<sup>+</sup> and I-B illustrates a rare positioning observed for some Li<sup>+</sup> with a Li<sup>+</sup>-carbonyl oxygen separation distance of about  $\sim$ 4 Å.

More quantitatively, Fig. 4 shows how the solvation shells and the atoms participating in the solvation shells were investigated using cumulative RDF (CRDF) plots while accounting for the dynamic electrolyte molecules. A simple example to illustrate the process is presented in Fig. S6 in the SI, calculated for a trajectory with a de-lithiated cathode with LiBF<sub>4</sub> salt showing the CRDF relative to the two Li<sup>+</sup> in the electrolyte region.

In Fig. 4, graphs I (DMC) and II (EC) show the frequencies with which an atoms are found at a given distance from the carbonyl oxygen of either DMC or EC summed up over the duration of the trajectory, shown here for a  $\text{LiPF}_6/\text{NiO}_2$  system. Graphs III and IV isolate the Li CRDF from graphs I and II, showing that the 2 Å peak in I and II is for a bond between the carbonyl oxygen and a  $\text{Li}^+$ . All other peaks coincide to intramolecular distances between the carbonyl oxygens and other atoms in either DMC or EC molecules, except for the two peaks at  $\sim$ 1.9-2.0 Å. Taken together with a visualization of the trajectory and after discounting for interactions with surface  $\text{Li}^+$ , the solvation shells of the

two Li<sup>+</sup> contain 3 EC and 1 DMC in one case and 1 EC and 2 DMC in the other. The summary of the number of EC and DMC molecules participating in the solvation shells around Li<sup>+</sup> is given in Fig. 5.

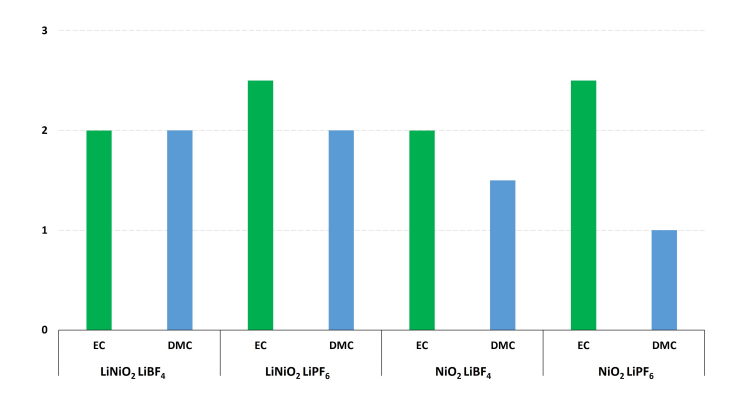


Figure 5: Summary of the average number of EC and DMC participating in a solvation shell for a  ${\rm Li^+}$  in each system.

In addition to these typical observations for all the systems, a peak at 4.0 Å for Li in the CRDF plot for DMC was seen to arise as the ether oxygen in the DMC also had a slight preference to participate in the shell relative to Li (orientation illustrated in the inset B of Fig 4-I). While infrequent, this was observed for some trajectories seemingly independent of the type of salt or the state of cathode lithiation. This orientation only prevailed for a brief period before turning to face the Li<sup>+</sup> with its carbonyl oxygen.

It was also seen that the carbonyl oxygen has a higher preference than the ether oxygen to participate in the shell in both EC and DMC molecules. This is due to the larger negative charge on the carbonyl oxygen relative to oxygens residing within a carbon chain [44]. Additionally, EC had a slightly higher chance of being in a shell relative to a DMC molecule in all the simulated systems (Fig. 5). Typically  $\sim$ 2 EC and  $\sim$ 1 DMC were observed to participate in a given shell, resulting in a total coordination of 2-3, whereas DFT calculations performed in a vacuum expects it to have 4 sites. This reduction with respect

to the number of coordination sites of Li<sup>+</sup> has more recently been reported to be tied to the presence of nearby anions which result in the change of tetrahedral symmetry of Li<sup>+</sup> coordination in concentrated EC electrolytes [19, 21]. Preferential solvation of Li<sup>+</sup> by cyclic and more polar molecules in the mixtures has also been previously reported, especially for EC over others, using *ab initio* and classical molecular dynamics simulations, atomic force microscopy and Raman spectroscopic studies, where the steric hindrances of cyclic molecules are overcome by stronger electrostatic interactions [44, 45, 46, 47, 22]. Additionally, it has been reported that in a low concentration electrolyte, the coordination of Li<sup>+</sup> is 4-6, while increasing the salt concentration results in a decrease to 1-2 sites, confirming our observations [22, 48]. Overall, the composition of the first solvation shell is now understood to be highly dependent on the form and polarity of the electrolyte, presence of nearby anions and the concentration of the salts.

The above discussion pertains to individual ion solvation shells. However, most solvation shells included both the cation and anion via the CIP structure (Fig. 1), essentially combining two solvation shells. While these superstructures were not always the same ratio of EC to DMC, the total number of molecules making up the first solvation shell remained consistent. By visual verification of trajectories, a total of eight molecules was determined to be the typical first solvation shell for both LiBF<sub>4</sub> and LiPF<sub>6</sub>. The orientation of molecules was also consistent for both salts. A total of three organic molecules were associated with the Li<sup>+</sup> of each salt (in addition to the BF<sub>4</sub><sup>-</sup> or PF<sub>6</sub><sup>-</sup>), typically the carbonyl oxygen facing the Li<sup>+</sup>. This leaves five molecules to surround the BF<sub>4</sub><sup>-</sup> or PF<sub>6</sub><sup>-</sup> side of the salt. These molecules showed a preference for the methylene or methyl groups to interact with the anion of the salt. However, we note that given the relatively shorter time scales accessible for ab initio molecular

dynamics trajectories, the results might vary for other shell formations which differ significantly from the starting CIP configurations of the salt.

### 3.2. Results from the DFT Calculations

During the charging and discharging process, solvation shells are formed and broken down at the cathode-electrolyte interface, respectively. Hence, for efficient charging and discharging of the battery, both the solvation and desolvation processes are important. The study of the energy involved in forming and breaking the first solvation shells is of particular interest, as it directly affects ion mobility and battery performance.

After the AIMD trajectories were run for at least 10 picoseconds, the formation and the orientation of the first solvation structure was studied visually. Once a general position was determined for a solvation shell from the AIMD trajectory, this was extracted as an initial solvation structure and used to create an input structure for DFT cluster analysis. An example for such a system can be seen in Fig. S7 in the SI.

Each molecule in the solvation structure was tested to see which had the weakest interaction. This was done by calculating the energy needed to remove each solvent molecule and then removing the particular solvent with the weakest interaction from the solvation shell (Eqn. 1),

$$E_{\text{Interaction}} = E_{\text{Cluster(n)}} - (E_{\text{Cluster(n-1)}} + E_{\text{Solvent}}),$$
 (1)

where  $E_{\text{Cluster(n)}}$  is the energy of the system where the solvent molecule in question is within the first solvation shell,  $E_{\text{Cluster(n-1)}}$  is the energy of the system without the solvent molecule in question, and  $E_{\text{Solvent}}$  is the energy of the isolated solvent molecule. Once the weakest interaction was identified, the solvent molecule was removed permanently and the structure was relaxed again.

This process was repeated to strip off each solvent molecule sequentially until only the salt remained.

The other method chosen to study each salt was to begin with an empty solvation structure (just the salt) and adding solvent molecules sequentially until a full first solvation shell was achieved. Relaxations were once again performed, followed by single point calculations, as described below. An EC molecule and a DMC molecule were each tested independently using Eqn. 1. The addition of the molecules at different sites was tested where the most energetically favorable structure was selected. The molecule at this particular favorable site was permanently added to the solvation structure, and the process was then repeated.

Initial structure relaxation was done using the B3PW91 method and 6-31G basis set, followed by a single point calculation with the B3PW91 functional [49], D3BJ dispersion correction with Becke-Johnson damping [50]), and a 6-311G++(d,p) basis set. The use of different basis sets for the relaxation and single point calculation was to limit the computational resources used. While AIMD and DFT methods used in the study used different functionals, their results are in agreement and complement each other.

The results from the calculations sequentially stripping or adding (starting from the empty salt anion) solvent molecules from the first solvation shell are summarized in Figs. 6 and 7 for (Li<sup>+</sup>)BF<sub>4</sub><sup>-</sup> and (Li<sup>+</sup>)PF<sub>6</sub><sup>-</sup>, respectively. The progress of the pathway, by way of addition/removal of molecules is shown by the horizontal (EC)/vertical (DMC) direction, together with the change in energy at each step.

#### 3.2.1. LiBF<sub>4</sub>

Beginning our discussion with the completed solvation structure taken from AIMD, it is seen in Fig. 6 that LiBF<sub>4</sub> had a first solvation shell of 2 DMC

and 6 EC. From the starting configuration (panel I of Fig. 6), we observed that the first three molecules removed from the structure are all EC, and they are removed from the BF<sub>4</sub><sup>-</sup> side of the salt pair. This is then followed by the removal of a DMC, then another EC, each also from the BF<sub>4</sub><sup>-</sup>. The last three molecules being removed all came from the Li<sup>+</sup>, since molecules bonded to the lithium have the strongest interaction energy, likely due to the marked difference in electronegativity between Li<sup>+</sup> and O. More importantly, the last remaining molecule was a DMC, indicating that the carbonyl oxygen from the DMC has a stronger interaction than the carbonyl oxygen of the EC. The cost of removing a solvent molecule ranges from 0.55 eV to 1.08 eV, with differences due to varying nearest neighbors, the number of remaining solvent molecules, and overall solvent-ion interactions.

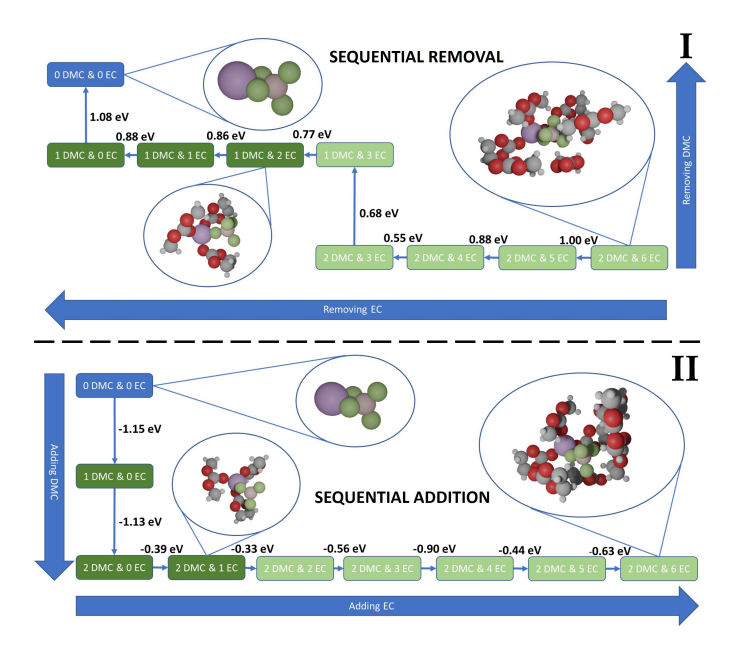


Figure 6: The lowest-energy pathway with which molecules were removed from (I) or added to (II) the solvation shell of LiBF<sub>4</sub>. The light (dark) green boxes indicate that the solvent molecule was removed/added from/to the BF<sub>4</sub> $^-$  (Li $^+$ ) side of the salt. The values on the arrows show the energy needed to remove/add from/to the molecule from the solvation shell. This energy was determined using the negative/positive of Eqn. 1.

The next approach to investigate the formation of the solvation shell began with an empty shell leading to the formation of a full first shell, which can be seen in the panel II of Fig. 6. We once again observe that the strongest interactions occur around the lithium, with the single strongest interaction being the addition of the initial DMC (-1.15 eV vs. -1.06 eV for EC). The energy gained with the addition of each solvent molecule ranges from 0.33 to 1.15 eV, depending on the solvent and the environment of the salt it associates with. The total number of DMC and EC added in this scenario are identical to what we started with (cluster taken from the AIMD trajectory), 2 DMC and 6 EC, seen in Fig. 6, albeit with slightly altered locations.

In these cluster simulations, we now have both DMC molecules interacting with the lithium, instead of just one. This difference may come from the size of the DMC molecules and the space available for movement. While the interaction energy with DMC is more favorable than with EC, Fig. 2 shows us that the methyl groups in the DMC molecule protrude perpendicular to the carbonyl oxygen. This may make it difficult for the molecule to align with the Li<sup>+</sup> once there is already another DMC bonded to the Li<sup>+</sup>, leaving room for the more compact EC to take its place. This steric effect was more evident in the AIMD simulations since the relaxation and single point method we used had free space surrounding the molecules; the dynamical nature treated with AIMD leaves less free space available in this manner. This highlights the importance of molecular dynamics in capturing the realistic solvation structures observed in experimental conditions.

# 3.2.2. LiPF<sub>6</sub>

The same process described in Sec. 3.2.1 was also performed for LiPF<sub>6</sub>. For this structure, we began with 4 DMC and 4 EC molecules in the solvation shell. Similar trends can be observed despite the difference in the initial amount of

DMC and EC from the LiBF<sub>4</sub> case (Sec. 3.2.1). The strongest interactions are still involving the Li<sup>+</sup>, as the final three molecules to be removed were around the Li<sup>+</sup>, as shown in Fig. 7. A DMC was also the last molecule remaining in the solvation shell. In this case, the cost of removing the first four solvent molecules was much less than for LiBF<sub>4</sub>, with values of 0.27, 0.44, 0.55, and 0.52 eV, yet the interaction energies are near 1 eV for the remaining solvent molecules, slightly higher than LiBF<sub>4</sub>.

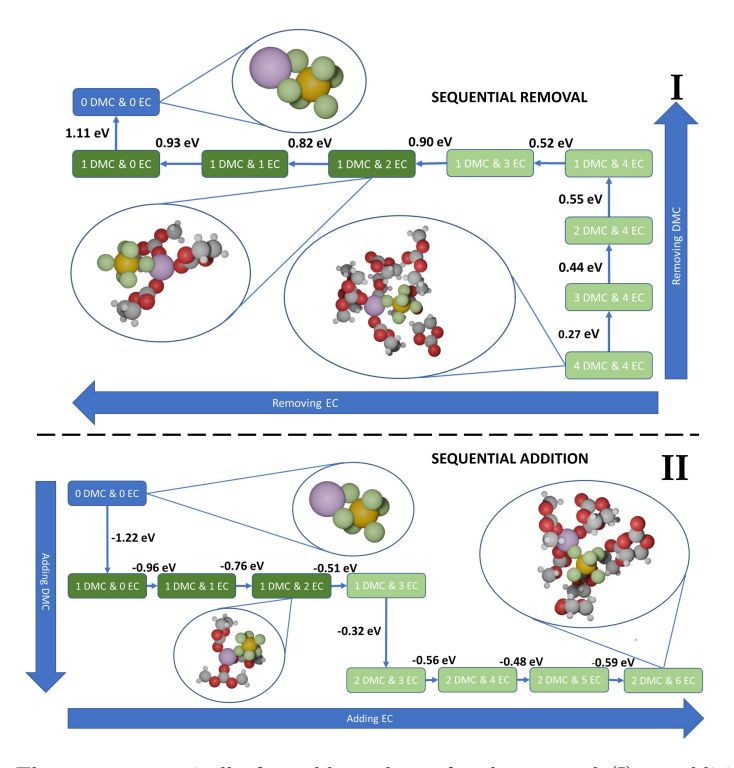


Figure 7: The most energetically favorable pathway for the removal (I) or addition (II) of molecules for the first solvation shell of LiPF<sub>6</sub>. The dark (light) green boxes indicate the solvent molecule was removed/added from/to the  ${\rm Li^+}~({\rm PF_6}^-)$ . The values on the arrows show the energy needed to remove/add from/to the molecule from the solvation shell. This energy was determined using the negative/positive of Eqn. 1.

Beginning from the empty structure, we still find similar trends, shown in the panel II of Fig. 7. The first molecule added to the structure is DMC, with the energy of addition of a DMC being -1.22 eV and EC -1.10 eV. The first three molecules all interact with the Li<sup>+</sup>, and the remaining molecules interact with PF<sub>6</sub><sup>-</sup>. With a full first solvation shell, there are 2 DMC and 6 EC, yielding a similar solvation shell to LiBF<sub>4</sub> (Fig. 6). Again, the interaction energy is somewhat weaker than it was for LiBF<sub>4</sub>, particularly for those solvent molecules interacting with the PF<sub>6</sub><sup>-</sup> anion. Evidently, the stripping of solvent molecules from LiPF<sub>6</sub> is easier than the stripping of solvent molecules from LiBF<sub>4</sub>, especially when interacting with the anion of the salt, which is understood to be due to the larger size of the PF<sub>6</sub><sup>-</sup> anion. The boron to fluorine distance for the BF<sub>4</sub><sup>-</sup> anion is lower by  $\sim$ 0.21 Å relative to PF<sub>6</sub><sup>-</sup> in the sequentially added solvation structures. Additionally, the next interaction of boron and phosphorous atoms in the CIP shell (ignoring the cation) is with hydrogens from EC and DMC at a distance of 2.98 Å and 3.12 Å for BF<sub>4</sub><sup>-</sup> and PF<sub>6</sub><sup>-</sup>, respectively (Fig. S8). This ease of stripping solvent molecules will allow for easier desolvation of the Li<sup>+</sup> as it enters either electrode [51, 52, 53].

In both the sequential addition and removals for LiBF<sub>4</sub> and LiPF<sub>6</sub> salts shown in Figs. 6 and 7, we see that the strongest interaction with the Li<sup>+</sup> ion is with a DMC molecule. The coordination of solvents to Li salts in electrolytes is influenced by several factors, including the solvent's dielectric constant, Lewis basicity, steric effects, and the presence of anions nearby. While EC has a higher relative permittivity and stronger Lewis basicity than DMC, these factors do not seem to necessarily dictate the strength of coordination. In our calculations, we observe that EC has a slightly higher preference to participate in the CIP shell compared to DMC in AIMD (Fig. 5). There are findings that have found Li<sup>+</sup> to bind more strongly with EC than with DMC in binary EC/DMC solvents (using electrospray ionization and mass spectrometry (ESI-MS)) [54]. This indicated a preference towards stronger ion dipole interactions between EC relative to DMC. However, their measurements have come from isolated

clusters with two solvent molecules instead of four, and with possible additional partial desolvation during measurements as a result of the experimental method. There are yet other findings that point out a slightly higher preference for the  ${\rm Li^+}$  to bind with DMC, with the difference in the composition of the  ${\rm Li^+}$  solvation being attributed to difference of calculations performed in the gas and liquid phases [55, 56, 57]. Further to that, in the works by Borodin and Smith above, and Ponnuchamy indicate that the presence of the  ${\rm PF_6}^-$  anion in the liquid electrolyte might strongly influence the relative stability of EC vs. DMC cation coordination, resulting in the modification of the tetrahedral structure of the  ${\rm Li^+}$  [58]. Consequentially, the overall charge of solvated structure of  ${\rm Li^+}$  is significantly reduced, thereby reducing the mobility of the solvation super structure in an applied potential. We also note, although the DMC molecule is the last to be removed from the CIP shells that were considered, the comparison of the energies for the last EC and the DMC molecules to be removed shows that the comparative difference between the two is minimal ( $\sim 0.1 \ {\rm eV}$ ) (Fig. S9).

#### 3.3. Solvent Separated Ion Pair

One more way that we tested our results for the determination of the number of molecules in the solvation structure was to split the salt into its individual components. By observing the interaction of each ion (Li<sup>+</sup>, BF<sub>4</sub><sup>-</sup>, PF<sub>6</sub><sup>-</sup>) with only EC or DMC, we were able to get a fuller description of the solvation structures. Looking at Fig. 8, we can see the solvation structures of the components of LiPF<sub>6</sub> when the ions are split apart. We notice the orientations of the molecules remain the same as when observed in Sec. 3.2.2, with the carbonyl oxygen of either EC or DMC interacting with the Li<sup>+</sup> ion, and the methyl or methylene group interacting with the PF<sub>6</sub><sup>-</sup>. This trend also holds for components of LiBF<sub>4</sub>, which has been excluded from Fig. 8 as the images are similar to those already shown.

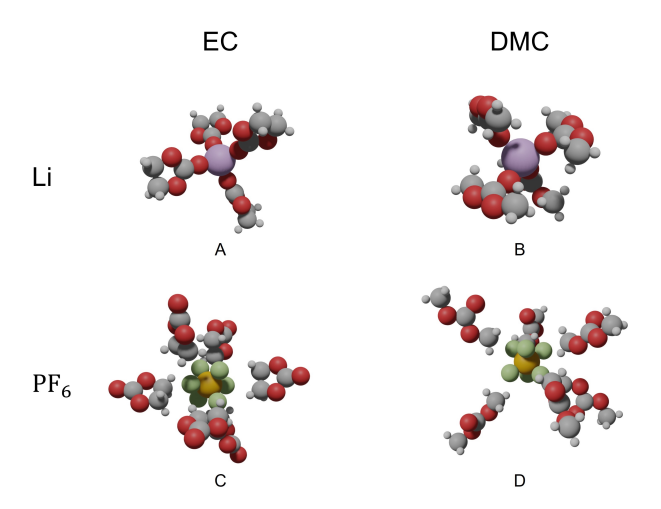


Figure 8: Solvation structures of the individual components of LiPF<sub>6</sub>. (A) Li<sup>+</sup> with four EC, (B) Li<sup>+</sup> with four DMC, (C) PF<sub>6</sub><sup>-</sup> with six EC, and (D) PF<sub>6</sub><sup>-</sup> with six DMC.

From these results, we also notice that the total number of molecules in the first solvation shell of lithium is four for either EC or DMC. This is consistent with what is found in the literature [56, 16, 17, 18]. The total number of molecules in the first solvation shell for both BF<sub>4</sub><sup>-</sup> and PF<sub>6</sub><sup>-</sup> was found to be six for either EC or DMC. These results are similar to those found by Chaban, who showed that the results for the anion are not entirely clear [16]. When the solvent molecules come together, we postulate that each component takes one available site away from the other's first solvation shell (Li<sup>+</sup> and the anion), giving us three molecules on the Li<sup>+</sup> and five molecules on the BF<sub>4</sub><sup>-</sup> or PF<sub>6</sub><sup>-</sup>, as we found in Sec. 3.2.1 and 3.2.2.

## 4. Conclusion

The dynamics of LiBF<sub>4</sub> and LiPF<sub>6</sub> salts in a 1:1 EC:DMC electrolyte both within the electrolyte as well as closer to lithiated and de-lithiated cathode surfaces were studied using AIMD. The pathways for the formation and disintegration of the first solvation shell around  ${\rm BF_4}^-$  or  ${\rm PF_6}^-$  anions were calculated

using DFT. The CIP solvation shells expressed a higher tendency to disintegrate near lithiated LiNiO<sub>2</sub> cathode surfaces compared to de-lithiated surfaces. EC generally contributed more to the solvation shell compared to DMC. From our results we observe that  $LiBF_4$  and  $LiPF_6$  have similar solvation structures and interaction energies. The molecules in the solvation structure showed a preference for the carbonyl oxygens and the ether oxygens to interact with Li<sup>+</sup>, and the methyl or methylene groups to interact with the  ${\rm BF_4}^-$  or  ${\rm PF_6}^-$ . Both salts had a total of eight molecules in the CIP solvation structure. While the first DMC molecules had a slightly stronger interaction with the lithium in LiPF<sub>6</sub> than in LiBF<sub>4</sub>, the energies were comparable, meaning that it is mostly the DMC initiating the formation of solvation shells. When dissociation of the solvation shell is considered, LiPF<sub>6</sub> can desolvate more easily compared to LiBF<sub>4</sub> by  $\sim 1$  eV. The orientations and the number of molecules participating in the first solvation shell were consistent for both salts. This investigation emphasized the important and complementary roles played by both DFT and AIMD, where DFT accurately captures energetics while AIMD captures dynamics and steric effects in the formation of solvation shells.

# Acknowledgments

This work was supported by the National Science Foundation under Grant No. CBET-2028722. This work was performed using *Expanse*, a part of the Extreme Science and Engineering Discovery Environment (XSEDE), which is supported by NSF Grant No. 1928224 under allocation TG-DMR180009 and *Spiedie* HPC at Binghamton University. We thank Dr. Louis Piper in the Electrochemical Materials Department at the University of Warwick for insightful discussions regarding this work.

#### References

- [1] L. Monconduit, R. Dedryvère, L. Croguennec, Electrodes for Li-ion Batteries, 1st Edition, Vol. 2, Wiley, 2015.
- [2] J. Young, P. M. Kulick, T. R. Juran, M. Smeu, Comparative Study of Ethylene Carbonate-Based Electrolyte Decomposition at Li, Ca, and Al Anode Interfaces, ACS Applied Energy Materials 2 (2019) 1676–1684. URL https://pubs.acs.org/doi/abs/10.1021/acsaem.8b01707
- [3] L. M. Rodriguez-Martinez, N. Omar, Emerging nanotechnologies in rechargeable energy storage systems, 1st Edition, Elsevier Inc., 2017. URL http://www.sciencedirect.com/science/article/pii/ B9780323429771000017
- [4] L. Hu, Z. Zhang, K. Amine, Electrochemical investigation of carbonate-based electrolytes for high voltage lithium-ion cells, Journal of Power Sources 236 (2013) 175-180. doi:10.1016/J.JPOWSOUR.2013.02.064. URL https://www.sciencedirect.com/science/article/abs/pii/S0378775313003492
- [5] K. Xu, Li-ion battery electrolytes, Nature Energy 6 (2021) 763. doi:10. 1038/s41560-021-00841-6.
   URL https://doi.org/10.1038/s41560-021-00841-6
- [6] Z. Hou, M. Dong, Y. Xiong, X. Zhang, Y. Zhu, Y. Qian, Formation of Solid-Electrolyte Interfaces in Aqueous Electrolytes by Altering Cation-Solvation Shell Structure, Advanced Energy Materials 10 (15) (2020) 1903665. doi:10.1002/aenm.201903665.
- [7] Z. Hu, L. Zhao, T. Jiang, J. Liu, A. Rashid, P. Sun, G. Wang, C. Yan, L. Zhang, Trifluoropropylene Carbonate-Driven Interface Regulation Enabling Greatly Enhanced Lithium Storage Durability of Silicon-Based Anodes, Advanced Functional Materials 29 (45) (2019) 1906548. doi: 10.1002/adfm.201906548.
- [8] L. Xing, X. Zheng, M. Schroeder, J. Alvarado, A. Von Wald Cresce, K. Xu, Q. Li, W. Li, Deciphering the Ethylene Carbonate-Propylene Carbonate Mystery in Li-Ion Batteries, Accounts of Chemical Research 51 (2) (2018) 282–289. doi:10.1021/acs.accounts.7b00474.
- [9] J. P. Pender, G. Jha, D. H. Youn, J. M. Ziegler, I. Andoni, E. J. Choi, A. Heller, B. S. Dunn, P. S. Weiss, R. M. Penner, C. B. Mullins, Electrode Degradation in Lithium-Ion Batteries, ACS Nano 14 (2) (2020) 1243–1295. doi:10.1021/ACSNAND.9B04365.
- [10] J. Tong, S. Wu, N. von Solms, X. Liang, F. Huo, Q. Zhou, H. He, S. Zhang, The Effect of Concentration of Lithium Salt on the Structural and Transport Properties of Ionic Liquid-Based Electrolytes, Frontiers in Chemistry

- 7 (2020). doi:10.3389/fchem.2019.00945. URL www.frontiersin.org
- [11] L. Zhang, Y. Chen, Electrolyte solvation structure as a stabilization mechanism for electrodes, Energy Materials (2021) 1-9doi:10.20517/energymater.2021.04.
- [12] J. Ming, Z. Cao, W. Wahyudi, M. Li, P. Kumar, Y. Wu, J.-Y. Hwang, M. Nejib Hedhili, L. Cavallo, Y.-K. Sun, L.-J. Li, S. Arabia, New Insights on Graphite Anode Stability in Rechargeable Batteries: Li Ion Coordination Structures Prevail over Solid Electrolyte Interphases, ACS Energy Letters 3 (2018) 335–340. doi:10.1021/acsenergylett.7b01177.
- [13] C. L. Berhaut, D. Lemordant, P. Porion, L. Timperman, G. Schmidt, M. Anouti, Ionic association analysis of LiTDI, LiFSI and LiPF6 in EC/DMC for better Li-ion battery performances, RSC Advances 9 (8) (2019) 4599-4608. doi:10.1039/C8RA08430K. URL https://pubs.rsc.org/en/content/articlelanding/2019/ra/c8ra08430k
- [14] Z. Chang, Y. Qiao, H. Deng, H. Yang, P. He, H. Zhou, A Liquid Electrolyte with De-Solvated Lithium Ions for Lithium-Metal Battery, Joule 4 (8) (2020) 1776-1789. doi:10.1016/j.joule.2020.06.011. URL https://www.sciencedirect.com/science/article/pii/ S2542435120302749
- [15] M. Takeuchi, N. Matubayasi, Y. Kameda, B. Minofar, S. I. Ishiguro, Y. Umebayashi, Free-energy and structural analysis of ion solvation and contact ion-pair formation of Li+ with BF4- and PF 6- in water and carbonate solvents, Journal of Physical Chemistry B 116 (22) (2012) 6476–6487. doi:10.1021/jp3011487.
- [16] V. Chaban, Solvation of the fluorine containing anions and their lithium salts in propylene carbonate and dimethoxyethane, Journal of Molecular Modeling 21 (172) (2015). doi:10.1007/s00894-015-2717-y.
- J.-C. Soetens, C. Millot, B. Maigret, Molecular Dynamics Simulation of Li+BF4- in Ethylene Carbonate, Propylene Carbonate, and Dimethyl Carbonate Solvents, The Journal of Physical Chemistry A 102 (7) (1998) 1055– 1061. doi:10.1021/jp972457+. URL https://doi.org/10.1021/jp972457+
- [18] G. Z. Tulibaeva, A. F. Shestakov, V. I. Volkov, O. V. Yarmolenko, Structure of LiBF4 Solvate Complexes in Ethylene Carbonate, Based on High-Resolution NMR and Quantum-Chemical Data, Russian Journal of Physical Chemistry A 92 (4) (2018) 625–632. doi:10.1134/S0036024418040313.
- [19] B. Jiang, V. Ponnuchamy, Y. Shen, X. Yang, K. Yuan, V. Vetere, S. Mossa, I. Skarmoutsos, Y. Zhang, J. Zheng, The anion effect on li+ ion coordination structure in ethylene carbonate solutions, The Journal of Physical

- Chemistry Letters 7 (18) (2016) 3554-3559. arXiv:https://doi.org/10.1021/acs.jpclett.6b01664, doi:10.1021/acs.jpclett.6b01664. URL https://doi.org/10.1021/acs.jpclett.6b01664
- [20] J. Self, K. D. Fong, K. A. Persson, Transport in Superconcentrated LiPF6 and LiBF4/Propylene Carbonate Electrolytes, ACS Energy Letters 4 (12) (2019) 2843–2849. doi:10.1021/acsenergylett.9b02118. URL https://doi.org/10.1021/acsenergylett.9b02118
- [21] I. Skarmoutsos, V. Ponnuchamy, V. Vetere, S. Mossa, Li <sup>+</sup> Solvation in Pure, Binary, and Ternary Mixtures of Organic Carbonate Electrolytes, The Journal of Physical Chemistry C 119 (9) (2015) 4502-4515. doi: 10.1021/jp511132c. URL https://pubs.acs.org/doi/10.1021/jp511132c
- [22] L. Su, X. Zhao, M. Yi, H. Charalambous, H. Celio, Y. Liu, A. Manthiram, Uncovering the Solvation Structure of LiPF 6 -Based Localized Saturated Electrolytes and Their Effect on LiNiO 2 -Based Lithium-Metal Batteries, Advanced Energy Materials 12 (36) (2022) 2201911. doi:10.1002/aenm.202201911. URL https://onlinelibrary.wiley.com/doi/10.1002/aenm.202201911
- [23] G. Kresse, J. Hafner, Norm-conserving and ultrasoft pseudopotentials for first-row and transition elements, Journal of Physics: Condensed Matter 6 (1994) 8245. doi:10.1088/0953-8984/6/40/015. URL https://iopscience.iop.org/article/10.1088/0953-8984/6/ 40/015
- [24] G. Kresse, J. Furthmüller, Efficiency of ab-initio total energy calculations for metals and semiconductors using a plane-wave basis set, Computational Materials Science 6 (1996) 15–50. doi:10.1016/0927-0256(96)00008-0.
- [25] G. Kresse, J. Furthmüller, Efficient iterative schemes for ¡i¿ab initio¡/i¿ total-energy calculations using a plane-wave basis set, Physical Review B 54 (16) (1996) 11169–11186. doi:10.1103/PhysRevB.54.11169. URL https://link.aps.org/doi/10.1103/PhysRevB.54.11169
- [26] G., J. Hafner, Norm-conserving and ultrasoft pseudopotentials for first-row and transition elements, Journal of Physics: Condensed Matter 6 (1994) 8245. doi:10.1088/0953-8984/6/40/015.
   URL https://iopscience.iop.org/article/10.1088/0953-8984/6/40/015
- [27] G. Kresse, D. Joubert, From ultrasoft pseudopotentials to the projector augmented-wave method, Physical Review B 59 (1999) 1758. doi:10.1103/PhysRevB.59.1758. URL https://journals.aps.org/prb/abstract/10.1103/PhysRevB.59.1758

- [28] J. P. Perdew, K. Burke, M. Ernzerhof, Generalized gradient approximation made simple, Physical Review Letters 77 (1996) 3865. doi:10.1103/PhysRevLett.77.3865. URL https://journals.aps.org/prl/abstract/10.1103/PhysRevLett.77.3865
- J. P. Perdew, K. Burke, M. Ernzerhof, Generalized gradient approximation made simple [phys. rev. lett. 77, 3865 (1996)], Physical Review Letters 78 (1997) 1396. doi:10.1103/PhysRevLett.78.1396.
   URL https://journals.aps.org/prl/abstract/10.1103/PhysRevLett.78.1396
- [30] J. D. Pack, H. J. Monkhorst, "Special points for Brillouin-zone integrations"—a reply, Physical Review B 16 (4) (1977) 1748–1749, publisher: American Physical Society. doi:10.1103/PhysRevB.16.1748. URL https://link.aps.org/doi/10.1103/PhysRevB.16.1748
- [31] H. J. Monkhorst, J. D. Pack, Special points for Brillouin-zone integrations, Physical Review B 13 (12) (1976) 5188-5192, publisher: American Physical Society. doi:10.1103/PhysRevB.13.5188. URL https://link.aps.org/doi/10.1103/PhysRevB.13.5188
- [32] A. Jain, S. P. Ong, G. Hautier, W. Chen, W. D. Richards, S. Dacek, S. Cholia, D. Gunter, D. Skinner, G. Ceder, K. A. Persson, Commentary: The materials project: A materials genome approach to accelerating materials innovation, APL Materials 1 (2013) 011002. doi:10.1063/1.4812323. URL https://aip.scitation.org/doi/abs/10.1063/1.4812323
- [33] A. Stukowski, Visualization and analysis of atomistic simulation data with ovito-the open visualization tool, Modelling and Simulation in Materials Science and Engineering 18 (2009) 015012. doi:10.1088/0965-0393/18/ 1/015012. URL https://iopscience.iop.org/article/10.1088/0965-0393/18/ 1/015012
- [34] K. Momma, F. Izumi, Vesta 3 for three-dimensional visualization of crystal, volumetric and morphology data, Journal of Applied Crystallography 44 (2011) 1272–1276. doi:10.1107/S0021889811038970. URL https://scripts.iucr.org/cgi-bin/paper?S0021889811038970
- [35] M. D. Hanwell, D. E. Curtis, D. C. Lonie, T. Vandermeerschd, E. Zurek, G. R. Hutchison, Avogadro: An advanced semantic chemical editor, visualization, and analysis platform, Journal of Cheminformatics 4 (2012) 17. doi:10.1186/1758-2946-4-17.
  URL https://jcheminf.biomedcentral.com/articles/10.1186/1758-2946-4-17
- [36] J. G. Lee, Computational Materials Science: An Introduction, 2nd Edition, CRC Press, 2016. URL https://books.google.com/books?id=4eiVDQAAQBAJ

- [37] K. Leung, First-principles modeling of the initial stages of organic solvent decomposition on li xmn 20 4(100) surfaces, Journal of Physical Chemistry C 116 (2012) 9852–9861. doi:10.1021/jp212415x.
- [38] B. Zhang, Z. Lin, H. Chen, L.-W. Wang, F. Pan, The stability and reaction mechanism of a LiF/electrolyte interface: insight from density functional theory, Journal of Materials Chemistry A 8 (5) (2020) 2613– 2617. doi:10.1039/C9TA10170E. URL https://pubs.rsc.org/en/content/articlelanding/2020/ta/ c9ta10170e
- [39] J. Young, M. Smeu, Preventing electrolyte decomposition on a ca metal electrode interface using an artificial solid-electrolyte interphase, Advanced Theory and Simulations 4 (8) (2021) 2100018. doi:10.1002/adts.202100018. URL https://onlinelibrary.wiley.com/doi/10.1002/adts. 202100018
- [40] S. Grimme, J. Antony, S. Ehrlich, H. Krieg, A consistent and accurate ab initio parametrization of density functional dispersion correction (dft-d) for the 94 elements h-pu, The Journal of Chemical Physics 132 (2010) 154104. doi:10.1063/1.3382344. URL https://aip.scitation.org/doi/abs/10.1063/1.3382344
- [41] J. Kang, B. Han, First-principles study on the thermal stability of linio2 materials coated by amorphous al2o3 with atomic layer thickness, ACS Applied Materials and Interfaces 7 (2015) 11599-11603. doi:10.1021/ACSAMI.5B02572/SUPPL\_FILE/AM5B02572\_SI\_001.PDF. URL https://pubs.acs.org/doi/abs/10.1021/acsami.5b02572
- [42] J. Le, M. Iannuzzi, A. Cuesta, J. Cheng, Determining potentials of zero charge of metal electrodes versus the standard hydrogen electrode from density-functional-theory-based molecular dynamics, Phys. Rev. Lett. 119 (2017) 016801. doi:10.1103/PhysRevLett.119.016801. URL https://link.aps.org/doi/10.1103/PhysRevLett.119.016801
- [43] M. D. Bhatt, M. Cho, K. Cho, Density functional theory calculations and ab initio molecular dynamics simulations for diffusion of li+ within liquid ethylene carbonate, Modelling and Simulation in Materials Science and Engineering 20 (2012) 065004. doi:10.1088/0965-0393/20/6/065004. URL https://iopscience.iop.org/article/10.1088/0965-0393/20/ 6/065004
- [44] O. O. Postupna, Y. V. Kolesnik, O. N. Kalugin, O. V. Prezhdo, Microscopic Structure and Dynamics of LiBF <sub>4</sub> Solutions in Cyclic and Linear Carbonates, The Journal of Physical Chemistry B 115 (49) (2011) 14563–14571. doi:10.1021/jp206006m.
  URL https://pubs.acs.org/doi/10.1021/jp206006m

- [45] M. Morita, Y. Asai, N. Yoshimoto, M. Ishikawa, A Raman spectroscopic study of organic electrolyte solutions based on binary solvent systems of ethylene carbonate with low viscosity solvents which dissolve different lithium salts, Journal of the Chemical Society, Faraday Transactions 94 (23) (1998) 3451-3456. doi:10.1039/A806278A. URL https://pubs.rsc.org/en/content/articlelanding/1998/ft/ a806278a
- [46] O. Borodin, M. Olguin, P. Ganesh, P. R. C. Kent, J. L. Allen, W. A. Henderson, Competitive lithium solvation of linear and cyclic carbonates from quantum chemistry, Physical Chemistry Chemical Physics 18 (1) (2016) 164-175. doi:10.1039/C5CP05121E. URL https://pubs.rsc.org/en/content/articlelanding/2016/cp/c5cp05121e
- [47] S.-K. Jeong, M. Inaba, Y. Iriyama, T. Abe, Z. Ogumi, Surface film formation on a graphite negative electrode in lithium-ion batteries: AFM study on the effects of co-solvents in ethylene carbonate-based solutions, Electrochimica Acta 47 (12) (2002) 1975–1982.
  URL https://linkinghub.elsevier.com/retrieve/pii/S0013468602000993
- [48] K. Xu, Electrolytes and Interphases in Li-Ion Batteries and Beyond, Chemical Reviews 114 (23) (2014) 11503-11618. doi:10.1021/cr500003w. URL https://pubs.acs.org/doi/10.1021/cr500003w
- [49] P. J. Stephen, F. J. Devlin, C. F. Chabalowski, M. J. Frisch, Ab Initio Calculation of Vibrational Absorption, The Journal of Physical Chemistry 98 (45) (1994) 11623–11627.
- [50] L. G. Stefan Grimme, Stephan Ehrlich, Effect of the damping function in dispersion corrected density functional theory, Journal of Computational Chemistry 32 (2011) 1456-1465. doi:10.1002/JCC.21759.
   URL https://onlinelibrary.wiley.com/doi/full/10.1002/jcc.21759
- [51] H. Moon, R. Tatara, T. Mandai, K. Ueno, K. Yoshida, N. Tachikawa, T. Yasuda, K. Dokko, M. Watanabe, Mechanism of li ion desolvation at the interface of graphite electrode and glyme-li salt solvate ionic liquids, The Journal of Physical Chemistry C 118 (35) (2014) 20246–20256. doi: 10.1021/jp506772f.
- [52] D. Kundu, S. H. Vajargah, L. Wan, B. Adams, D. Prendergast, L. F. Nazar, Aqueous vs. nonaqueous Zn-ion batteries: consequences of the desolvation penalty at the interface<sup>†</sup>, Energy and Environmental Science 11 (2018) 881– 892. doi:10.1039/c8ee00378e.

- [53] L. F. Wan, B. R. Perdue, C. A. Apblett, D. Prendergast, Mg Desolvation and Intercalation Mechanism at the Mo<sub>6</sub>S<sub>8</sub> Chevrel Phase Surface, Chemistry of Materials 27 (2015) 5932-5940. doi:10.1021/acs.chemmater. 5b01907.
- [54] A. von Cresce, K. Xu, Preferential solvation of li+ directs formation of interphase on graphitic anode, Electrochemical and Solid-State Letters 14 (10) (2011) A154. doi:10.1149/1.3615828. URL https://dx.doi.org/10.1149/1.3615828
- [55] O. Borodin, G. D. Smith, Quantum chemistry and molecular dynamics simulation study of dimethyl carbonate: Ethylene carbonate electrolytes doped with lipf6, The Journal of Physical Chemistry B 113 (6) (2009) 1763-1776, pMID: 19146427. doi:10.1021/jp809614h. URL https://doi.org/10.1021/jp809614h
- [56] M. Takeuchi, N. Matubayasi, Y. Kameda, B. Minofar, S.-i. Ishiguro, Y. Umebayashi, Free-energy and structural analysis of ion solvation and contact ion-pair formation of li+ with bf4- and pf6- in water and carbonate solvents, The Journal of Physical Chemistry B 116 (22) (2012) 6476-6487, pMID: 22616851. doi:10.1021/jp3011487. URL https://doi.org/10.1021/jp3011487
- [57] O. Borodin, Molecular modeling of electrolytes, Modern Aspects of Electrochemistry 58 (2014) 371–395. doi:10.1007/978-1-4939-0302-3\_8.
- [58] V. Ponnuchamy, S. Mossa, I. Skarmoutsos, Solvent and salt effect on lithium ion solvation and contact ion pair formation in organic carbonates: A quantum chemical perspective, The Journal of Physical Chemistry C 122 (45) (2018) 25930-25939. doi:10.1021/acs.jpcc.8b09892. URL https://doi.org/10.1021/acs.jpcc.8b09892